Dynamics of randomly branched polymers: Configuration averages and solvable models

F. Jasch, Ch. von Ferber, and A. Blumen
Theoretische Polymerphysik, Universität Freiburg, Hermann-Herder-Strasse 3, D-79104 Freiburg, Germany
(Received 9 June 2003; published 25 November 2003)

Treating the relaxation dynamics of an ensemble of random hyperbranched macromolecules in dilute solution represents a challenge even in the framework of Rouse-type approaches, which focus on generalized Gaussian structures (GGSs). The problem is that one has to average over a large class of realizations of molecular structures, and that each molecule undergoes its own dynamics. We show that a replica formalism allows to develop analytically, based on an integral equation, a systematic way to determine the ensemble averaged eigenvalue spectrum. Interestingly, for a specific probability distribution of the spring strengths of the GGSs, the integral equation takes a particularly simple form. Given that several dynamical observables, such as the mechanical moduli $G'(\omega)$ and $G''(\omega)$, as well as the averaged monomer displacement $\langle Y(t)\rangle$ are relatively simple functions of the eigenvalues, we can use the obtained spectra to compute the corresponding averaged dynamical forms. Comparing the results obtained from this approach and from extensive diagonalizations of hyperbranched GGSs we find a very good agreement.

DOI: 10.1103/PhysRevE.68.051106 PACS number(s): 46.65.+g, 82.70.Gg, 64.60.Ht, 83.80.Rs

I. INTRODUCTION

Randomly branched polymers and in particular their dynamic behavior have recently attracted much interest. On the theoretical side, this is due to the treelike structure of such polymers, which simplifies their treatment compared to complex networks, and to the quest for understanding the dynamical observables of such random networks [1–10]. On the experimental side, methods have been developed to synthesize large (regular as well as irregular) branched polymeric structures, i.e., dendrimers and their hyperbranched analoga [11–22].

While theoretical work on the dynamics of regular branched dendrimers has made use of the high symmetry of these molecules to extract (as far as possible in closed form) expressions for their eigenvalue spectra [10,23], for general hyperbranched polymers the corresponding spectra have been so far evaluated only using simulation and numerical diagonalization techniques [7]. In such approaches large ensembles of branched structures are generated; then the eigenfrequency spectra of the structures are determined, from which then averaged dynamical observables are calculated. We note that at long times the relaxation is dominated by the lowest eigenfrequencies of all contributing structures; these eigenfrequencies belong, as a rule, to the most elongated structures in the ensemble, structures which are rare. Evidently, in an ensemble built by simulating a finite number of elements, the statistics of rare events prevents one from obtaining accurately the very low part of the spectrum. Hence, the limiting long-time behavior of the dynamical relaxation forms cannot be obtained in this way.

In this work we focus on another approach, based on the analytical ideas of Kim and Harris [24] and of Bray and Rodgers [25]. Extending the analysis of gel dynamics by Broderix *et al.* [26] we obtain an integral equation for the eigenfrequencies of hyperbranched structures.

II. MODEL

A. The structures

Each representative of the ensemble of randomly branched structures is constructed from a single monomer to which one tries to attach with probability p a bond that ends at a new monomer. This attempt to add a bond is repeated f times, so that the number of bonds added to the starting monomer obeys a binomial distribution where f is the maximum number of possible bonds added to one monomer. In the next step the procedure of trying to add a bond ending at a new monomer is repeated $f-1$ times with each monomer created in each step. Proceeding iteratively in the same way with the monomers created in the last step, we obtain a randomly branched loopless structure. The process of adding bonds ends if no bonds are added in a given step. This event occurs with probability 1 below the percolation threshold $p_c=1/(f-1)$ [27–29], but for $p>p_c$ there is a finite probability that the process never stops and an infinite structure is created.

B. Dynamics

In this section we recall the evaluation of the dynamical properties of polymers in the framework of generalized Gaussian structures (GGSs) [30], an extension of the Rouse model [31]. GGSs are obtained by viewing the vertices of the structure as beads and the branches as entropic harmonic springs. The beads are then treated as Brownian particles characterized by their time dependent positions $\hat{\mathbf{r}}_i(t)$. The potential due to the harmonic springs with elastic constant K is

$$U(\{\hat{\mathbf{r}}_i\})=\frac{K}{2}\sum_{i<j} C_{ij}(\hat{\mathbf{r}}_i-\hat{\mathbf{r}}_j)^2=\frac{K}{2}\sum_{i,j} A_{ij}\hat{\mathbf{r}}_i\hat{\mathbf{r}}_j . \qquad (1)$$

In a classical picture [30–33] the symmetric matrix $\mathbf{C}=(C_{ij})$ indicates the connections: the off-diagonal elements C_{ik} are

either 1 if i and j are connected or 0 otherwise, and the diagonal elements C_{ii} are zero. Furthermore, the positive semidefinite Laplace operator $\mathbf{A}=(A_{ik})$ of the structure is given by

$$A_{ik}=\left(\delta_{ik}\sum_{j=1}^{N} C_{jk}\right)-C_{ik}. \tag{2}$$

Later, in order to obtain a solvable equation for the eigenfrequencies we will also generalize the potential given by Eq. (1) by letting the strength of the springs' constants vary over the lattice. Formally we will allow the nonzero values of C_{ik} to vary by picking them independently of each other from a probability density distribution $D(x)$, in the spirit of quenched disorder.

We consider purely relaxational dynamics in the presence of an external space and time dependent field $\mathbf{F}(\hat{\mathbf{r}},t)$. Thus the time dependence of the bead positions $\hat{\mathbf{r}}_i(t)$ is given by the Langevin equation

$$\zeta\frac{\partial\hat{\mathbf{r}}_i(t)}{\partial t}=-K\sum_{j=1}^{N} A_{ij}\hat{\mathbf{r}}_j+\mathbf{F}(\hat{\mathbf{r}}_i,t)+\mathbf{f}_i(t), \tag{3}$$

where $\mathbf{f}_i(t)$ denote random forces with zero mean and satisfying $\langle\mathbf{f}_i^T(t')\mathbf{f}_j(t)\rangle=2k_BT\zeta\delta_{ij}\delta(t-t')\mathbf{1}$, where ζ is the friction coefficient and T is the temperature. Equation (3) is the direct GGS generalization of the classical Rouse equation for linear polymers to networks [5,30,32].

From Eq. (3) various quantities can be calculated, which involve for a certain structure S only the density of eigenvalues $\rho_S(\lambda)$ of the corresponding Laplace matrix $\mathbf{A}^S$. Now, the ensemble averaged density of eigenvalues is given by

$$\rho(\lambda)=\langle\rho_S(\lambda)\rangle\equiv\sum_S w_S\rho_S(\lambda), \tag{4}$$

where the sum extends over all structures S, each $\rho_S(\lambda)$ is normalized, and w_S denotes the probability that the structure S is created in the iterative growth procedure.

Now each S created in this way is connected, so that A^S has only one zero eigenvalue, whose corresponding eigenvector is homogeneous. Therefore it is convenient to split off the resulting δ peak of $\rho(\lambda)$ at $\lambda=0$ with weight ρ_0 by writing

$$\rho(\lambda)=\rho_0\delta(\lambda)+\rho_+(\lambda). \tag{5}$$

If we consider the force $\mathbf{F}(\hat{\mathbf{r}}_j,t)=\delta_{ij}\Theta(t)\mathbf{F}$ acting only on bead i and switched on at $t=0$, we obtain for the mean bead displacement at time t, averaged over the fluctuating forces, all beads and the ensemble of structures, see Ref. [5]:

$$\overline{\hat{\mathbf{r}}(t)-\hat{\mathbf{r}}(0)}=\mathbf{F}\frac{\rho_0 t}{\zeta}+\mathbf{F}\frac{1}{K}\int_0^\infty d\lambda\rho_+(\lambda)\frac{1-\exp(-\lambda t/\tau)}{\lambda}, \tag{6}$$

where we set $\tau=\zeta/K$. We are also interested in the shear stress σ_{xy} which is obtained by having the force field $\mathbf{F}(\hat{\mathbf{r}},t)$ being proportional to a velocity field, which increases linearly in the y direction:

$$F_\alpha(\hat{\mathbf{r}},t)=\zeta v_\alpha(\hat{\mathbf{r}},t)=\zeta\delta_{\alpha x}\kappa(t)r_y. \tag{7}$$

In this case σ_{xy} is determined by the linear response relation [32]

$$\sigma_{xy}=\int_{-\infty}^{t} dt'\,\overline{G}(t-t')\kappa(t), \tag{8}$$

where the ensemble averaged shear relaxation modulus $\overline{G}(t)$ is given by

$$\overline{G}(t)=\hat{n}k_BT\int_0^\infty d\lambda\rho_+(\lambda)\exp(-2\lambda t/\tau), \tag{9}$$

and $\hat{n}\equiv N/V$ denotes the number of monomers per unit volume. For $\kappa(t)=\kappa$, independent of t, the intrinsic viscosity $\eta=\sigma_{xy}/\kappa$ reads

$$\eta=\hat{n}k_BT\frac{\tau}{2}\int_0^\infty d\lambda\frac{\rho_+(\lambda)}{\lambda}, \tag{10}$$

being again a function of $\rho_+(\lambda)$. The same holds when the external field is oscillatory, say by having $\kappa(t)=\kappa_0 e^{i\omega t}$; this leads to the storage modulus $G'(\omega)$:

$$G'(\omega)=\mathrm{Re}\left(\frac{\sigma_{xy}(t)i\omega e^{-i\omega t}}{\kappa_0}\right)=\hat{n}k_BT\int_0^\infty d\lambda\rho_+(\lambda)\frac{\omega^2}{(2\lambda/\tau)^2+\omega^2}, \tag{11}$$

and to the loss modulus $G''(\omega)$:

$$G''(\omega)=\mathrm{Im}\left(\frac{\sigma_{xy}(t)i\omega e^{i\omega t}}{\kappa_0}\right)=\hat{n}k_BT\int_0^\infty d\lambda\rho_+(\lambda)\frac{2\lambda\omega/\tau}{(2\lambda/\tau)^2+\omega^2}. \tag{12}$$

III. ANALYTIC TREATMENT VIA AN INTEGRAL EQUATION

A. Derivation of an integral equation for the density of states

We now turn to the derivation of an integral equation for the density of states, and follow the ideas developed by Kim and Harris [24] to treat random hopping over a Cayley tree.

We note that the construction of Sec. II A is not changed if we place the monomers from which our structures are built on the nodes of an f-functional Cayley tree and fill in the bonds, with probability p, in the order of increasing chemical distance from the starting monomer 0 at the origin. On the other hand, we may draw the bonds in arbitrary order, given that their probabilities of appearing are independent. There-

fore w_S defined in Sec. II A is the same as the probability of finding the origin to belong to an S cluster in the bond diluted Cayley tree. Due to the symmetry of the Cayley tree this probability is also independent of the choice of any particular monomer as being the origin.

We consider now in the diluted Cayley tree picture for a particular monomer j the diagonal element $R_{jj}(\lambda)=R(\lambda)$ of the resolvent $\mathbf{R}(\lambda)=\langle(\mathbf{A}^C-\lambda\mathbf{1})^{-1}\rangle$, averaged over all bond distributions:

$$R(\lambda)=\langle(\mathbf{A}^C-\lambda\mathbf{1})^{-1}_{jj}\rangle. \tag{13}$$

A particular realization C of the Cayley tree for a certain placement of bonds is formed by disjoint clusters of beads, a cluster being a set of beads connected to each other by bonds. Because of this the $\mathbf{A}^C$ corresponding to C can be written in block diagonal form, with block matrices given by the $\mathbf{A}^S$ of the corresponding clusters. One has therefore

$$(\mathbf{A}^C-\lambda\mathbf{1})^{-1}_{jj}=(\mathbf{A}^S-\lambda\mathbf{1})^{-1}_{jj}, \tag{14}$$

where S consists only of the monomers belonging to the cluster of j. Furthermore, the probabilities $w_{k,S}$ that a certain monomer is at a certain position k of S do not depend on k; one has thus $w_{k,S}=w_S/|S|$, where $|S|$ denotes the number of monomers inside S. This leads to

$$\begin{aligned}R(\lambda)&=\sum_S\sum_{k=1}^{|S|}w_{k,S}(\mathbf{A}^S-\lambda\mathbf{1})^{-1}_{kk}\\&=\sum_S w_S\frac{1}{|S|}\sum_{k=1}^{|S|}(\mathbf{A}^S-\lambda\mathbf{1})^{-1}_{kk}.\end{aligned} \tag{15}$$

Using the relation

$$\rho_S(\lambda)=\lim_{\epsilon\to0}\frac{1}{\pi}\frac{1}{|S|}\mathrm{Im}\sum_{k=1}^{|S|}[\mathbf{A}^S-(\lambda+i\epsilon)\mathbf{1}]^{-1}_{kk} \tag{16}$$

for the normalized density of states of the S cluster, we obtain from Eq. (4)

$$\rho(\lambda)=\lim_{\epsilon\to0}\frac{1}{\pi}\mathrm{Im}R(\lambda+i\epsilon), \tag{17}$$

with $R(\lambda)$ being given by Eq. (13). In fact, due to the symmetries mentioned, one can choose for j the origin

$$R(\lambda)=\langle(\mathbf{A}^C-\lambda\mathbf{1})^{-1}_{00}\rangle. \tag{18}$$

Now, the average over the disorder can be performed with the help of the replica method [34]. We recall first the Gaussian integral [35] valid for a particular C realization,

$$\begin{aligned}&\exp\left[\frac{i}{2}(\mathbf{A}^C-\lambda\mathbf{1})^{-1}_{00}J^2\right]\\&=\left[\mathrm{Det}\frac{i(\mathbf{A}^C-\lambda\mathbf{1})}{2\pi}\right]^{1/2}\int\left(\prod_j dx_j\right)\\&\quad\times\exp\left[-\frac{i}{2}\left(\sum_{j,k}A^C_{jk}x_jx_k-\lambda\sum_j x_j^2\right)+iJx_0\right],\end{aligned} \tag{19}$$

where λ contains implicitly a small, positive imaginary part which ensures the convergence. One now introduces the n-dimensional vector $\mathbf{J}=(J^{(1)},J^{(2)},\ldots,J^{(n)})$ and focuses on

$$Z(\mathbf{J})\equiv\exp\left[\frac{i}{2}(\mathbf{A}^C-\lambda\mathbf{1})^{-1}_{00}\mathbf{J}^2\right]. \tag{20}$$

Using Eq. (19) $Z(\mathbf{J})$ can be written as a Gaussian integral over the n-dimensional vectors $\mathbf{r}_i=(x_i^{(1)},x_i^{(2)},\ldots,x_i^{(n)})$:

$$\begin{aligned}Z(\mathbf{J})&=\left[\mathrm{Det}\frac{i(\mathbf{A}^C-\lambda\mathbf{1})}{2\pi}\right]^{n/2}\int\left(\prod_j d\mathbf{r}_j\right)\\&\quad\times\exp\left[-\frac{i}{2}\left(\sum_{j,k}A^C_{jk}\mathbf{r}_j\mathbf{r}_k-\lambda\sum_j\mathbf{r}_j^2\right)+i\mathbf{J}\cdot\mathbf{r}_0\right].\end{aligned} \tag{21}$$

In the spirit of the replica method, Eq. (18) can be expressed in terms of $Z(\mathbf{J})$ of Eq. (20) as

$$R(\lambda)=\left\langle\frac{-i}{n}\sum_{\alpha=1}^{n}\left(\frac{\partial}{\partial J^{(\alpha)}}\right)^2Z(\mathbf{J})\right|_{\mathbf{J}=\mathbf{0}}\Bigg\rangle, \tag{22}$$

where the average goes over all bond placements over the Cayley tree. Introducing Eq. (21) into Eq. (22) results in

$$\begin{aligned}R(\lambda)&=\left\langle\left[\mathrm{Det}\frac{i(\mathbf{A}^C-\lambda\mathbf{1})}{2\pi}\right]^{n/2}\frac{i}{n}\int\left(\prod_j d\mathbf{r}_j\right)\mathbf{r}_0^2\right.\\&\quad\left.\times\exp\left[-\frac{i}{2}\left(\sum_{j,k}A^C_{jk}\mathbf{r}_j\mathbf{r}_k-\lambda\sum_j\mathbf{r}_j^2\right)\right]\right\rangle.\end{aligned} \tag{23}$$

The averaging procedure in this equation is considerably simplified by taking the limit $n\to0$, since then the $(n/2)$th power of the determinant gives simply a factor 1.

Using Eq. (1) and the fact that the filling of bonds with probability p occurs independently leads to

$$\begin{aligned}R(\lambda)&\doteq\frac{i}{n}\int\left(\prod_j d\mathbf{r}_j\right)\mathbf{r}_0^2\exp\left[i\frac{\lambda}{2}\sum_j\mathbf{r}_j^2\right]\\&\quad\times\left\langle\exp\left[-\frac{i}{2}\sum_{j<k}C_{jk}(\mathbf{r}_j-\mathbf{r}_k)^2\right]\right\rangle\\&\doteq\frac{i}{n}\int\left(\prod_j d\mathbf{r}_j\right)\mathbf{r}_0^2\exp\left[i\frac{\lambda}{2}\sum_j\mathbf{r}_j^2\right]\prod_{\{j,k\}\epsilon B}F(\mathbf{r}_j,\mathbf{r}_k).\end{aligned} \tag{24}$$

Here we use the dot over the equation sign to indicate that the limit $n \to 0$ has to be taken. In Eq. (24) the product $\Pi_{\{j,k\}}$ runs over all the bonds $\{j,k\}$ of the Cayley tree; furthermore, setting $q=1-p$ we have defined

$$F(\mathbf{r}_j,\mathbf{r}_k) \equiv q + p \exp\left[-\frac{i}{2}(\mathbf{r}_j - \mathbf{r}_k)^2 \right]. \tag{25}$$

In fact one can also extend the present model, by also allowing [26] the strength of each bond to be weighted according to the normalized coupling strength distribution $D(\mu)$. In this case the generalized $F(\mathbf{r}_j,\mathbf{r}_k)$ is

$$F(\mathbf{r}_j,\mathbf{r}_k) \equiv q + p \int_0^\infty d\mu D(\mu) \exp\left[-i\frac{\mu}{2}(\mathbf{r}_j - \mathbf{r}_k)^2 \right]. \tag{26}$$

We now use the structure of the Cayley tree to perform the $\mathbf{r}_k$ integrations recursively in the generation number g of beads. We do this by integrating $\mathbf{r}_k$ of generation g, while taking its neighbor $\mathbf{r}_j$ of generation $g-1$ fixed [24].

For a tree of generation $g=1$ with coordination number $f=3$ one obtains in this way

$$\begin{aligned} R^{(1)}(\lambda) &\doteq \frac{i}{n}\int d\mathbf{r}_0 \mathbf{r}_0^2 \left(\exp\left[i\frac{\lambda}{2}\mathbf{r}_0^2 \right] \right) \\ &\quad \times \left(\int d\mathbf{r}_1 F(\mathbf{r}_0,\mathbf{r}_1) \exp\left[i\frac{\lambda}{2}\mathbf{r}_1^2 \right] \right) \\ &\quad \times \left(\int d\mathbf{r}_2 F(\mathbf{r}_0,\mathbf{r}_2) \exp\left[i\frac{\lambda}{2}\mathbf{r}_2^2 \right] \right) \\ &\quad \times \left(\int d\mathbf{r}_3 F(\mathbf{r}_0,\mathbf{r}_3) \exp\left[i\frac{\lambda}{2}\mathbf{r}_3^2 \right] \right) \\ &\doteq \frac{i}{n}\int d\mathbf{r}_0 \mathbf{r}_0^2 \left(\exp\left[i\frac{\lambda}{2}\mathbf{r}_0^2 \right] \right) \{\hat{\phi}^{(1)}(\mathbf{r}_0)\}^3, \end{aligned} \tag{27}$$

while in the general case of a tree of generation g with coordination number f one has [24]

$$R^{(g)}(\lambda) \doteq \frac{i}{n}\int d\mathbf{r} \mathbf{r}^2 \left(\exp\left[i\frac{\lambda}{2}\mathbf{r}^2 \right] \right) \{\hat{\phi}^{(g)}(\mathbf{r})\}^f, \tag{28}$$

where $\hat{\phi}^{(g)}(\mathbf{r})$ is determined recursively by

$$\hat{\phi}^{(g)}(\mathbf{r}) = \int d\mathbf{r}' F(\mathbf{r},\mathbf{r}') \left(\exp\left[i\frac{\lambda}{2}\mathbf{r}' \right] \right) \{\hat{\phi}^{(g-1)}(\mathbf{r}')\}^{f-1}, \tag{29}$$

with $\hat{\phi}^{(0)}(\mathbf{r}) \equiv 1$.

The $n \to 0$ limit is described in Appendix A and leads for a tree of generation g to the equations

$$R^{(g)}(\lambda) = -\frac{1}{\lambda}\int_0^\infty dx e^{-x} \{\phi^{(g)}(x)\}^f \tag{30}$$

and

$$\phi^{(g)}(x) = q + p\hat{\mathbf{O}} e^{-x} \{\phi^{(g-1)}(x)\}^{f-1}. \tag{31}$$

Here $\hat{\mathbf{O}}$ is the linear operator,

$$\hat{\mathbf{O}} = \int_0^\infty d\mu D(\mu) \exp\left[-\frac{\lambda}{\mu} x\partial_x^2 \right] = \sum_{k=0}^\infty \frac{\langle \mu^{-k} \rangle_\mu}{k!} (-\lambda)^k (x\partial_x^2)^k, \tag{32}$$

where $\langle \cdots \rangle_\mu$ denotes the average over the distribution $D(\mu)$. For an infinite Cayley tree the recursion relations take the form of a single integral equation of the function $\phi(x) \equiv \lim_{g\to\infty} \phi^{(g)}(x)$:

$$\phi(x) = q + p\hat{\mathbf{O}} e^{-x} \{\phi(x)\}^{f-1}, \tag{33}$$

where

$$R(\lambda) = -\frac{1}{\lambda}\int_0^\infty dx e^{-x} \{\phi(x)\}^f. \tag{34}$$

At this point we like to mention that treating hydrodynamic interactions (HI) in this formalism is fraught with problems. As shown in previous work [6,7] HI do indeed influence, in a marked way, the theoretical explanation of experimental observables. However, introducing the HI in the preaveraged approximation requires the determination of the eigenvalues of the matrix **HA** where the coefficients H_{ij} of **H** have the form

$$H_{ij} = \delta_{ij} + \zeta_r \frac{1-\delta_{ij}}{\sqrt{\langle (\hat{\mathbf{r}}_i - \hat{\mathbf{r}}_j)^2/l^2 \rangle}}, \tag{35}$$

with ζ_r being the reduced friction coefficient and l the mean square length of a bond. Now $\langle (\hat{\mathbf{r}}_i - \hat{\mathbf{r}}_j)^2/l^2 \rangle = (\mathbf{A}^{-1})_{ii} - 2(\mathbf{A}^{-1})_{ij} + (\mathbf{A}^{-1})_{jj}$, which renders clear that the A_{ij} enter **HA** in a complicated nonlinear form which does not allow a treatment along the lines used above.

If one lets f tend to infinity while keeping the average number $2c = pf$ of links attached to a given bead fixed, one recovers the results for the random graph discussed in Refs. [25,26]. This is seen from Eq. (33) by setting $g(\rho) \equiv 2c + \{\phi(-i\lambda\rho^2/2) - 1\} f$ so that Eq. (33) takes in the limit $f \to \infty$ the form

$$\begin{aligned} g(\rho) &= 2ce^{-2c} \int_0^\infty d\mu D(\mu) \exp\left[\frac{1}{2i\mu} \left(\partial_\rho^2 - \frac{1}{\rho}\partial_\rho \right) \right] \\ &\quad \times \exp\left[\frac{i\lambda}{2}\rho^2 + g(\rho) \right], \end{aligned} \tag{36}$$

which is identical with Eq. (A3) of Ref. [26].

Of special interest is the case $D(\mu) = \delta(\mu - 1)$, where $\hat{\mathbf{O}}$ is simply $\hat{\mathbf{O}} = \exp(-\lambda x \partial_x^2)$, see Eq. (32). It is possible now to obtain recursively $\phi^{(g)}(x)$ of the bond diluted Cayley tree of finite generation g based on Eq. (31). As shown in Appendix B one has then

$$\hat{\mathbf{O}} e^{ax} = \exp[ax/(1+\lambda a)]. \tag{37}$$

Indeed starting from $\phi^{(0)}(x)=1$ we obtain from Eqs. (37) and (31)

$$\phi^{(1)}(x)=q+p\exp[-x/(1-\lambda)]. \tag{38}$$

This can be again inserted into Eq. (31) to obtain $\phi^{(2)}(x)$. Iterating the procedure one obtains $\phi^{(g)}(x)$ as a sum over exponentials and, based on Eq. (30), it follows that $R^{(g)}(\lambda)$ is a rational function of λ. This procedure is, however, difficult to extend to large g, since the number of terms in $\phi^{(g)}(x)$ increases rapidly.

B. Moments of the density of eigenvalues

From Eq. (15) it is evident that $R(\lambda)$ diverges only for real, non-negative values. Hence in Cauchy's integral formula,

$$R(\lambda)=\frac{1}{2\pi i}\int_{C_\lambda} d\lambda' \frac{R(\lambda')}{\lambda'-\lambda}, \tag{39}$$

the closed path C_λ may be taken to wrap around the positive real axis and extend over a circle at infinity. Given that the integral over the circle does not contribute and making use of Eqs. (17) and (5) it follows that

$$R(\lambda)=-\frac{\rho_0}{\lambda}+\int_{0^+}^{\infty} d\lambda' \frac{\rho_+(\lambda')}{\lambda'-\lambda}. \tag{40}$$

One can now formally expand the denominator of Eq. (40) in powers of λ obtaining

$$R(\lambda)=-\frac{\rho_0}{\lambda}+\sum_{k=0}^{\infty}\lambda^k R_k, \tag{41}$$

with

$$R_k=\int_0^{\infty} d\lambda' \rho_+(\lambda')(\lambda')^{-k-1}. \tag{42}$$

If all the R_k exist, Eq. (42) represents an asymptotic expansion for $R(\lambda)$. Now, the R_k have physical meanings. For example, by Eq. (10), R_0 is related to the intrinsic viscosity:

$$\eta=\hat{n}k_BT\frac{\tau}{2}R_0, \tag{43}$$

while R_1, the second inverse moment, is related to the slope of $G'(\omega)$ at $\omega=0$ via

$$R_1=\frac{\tau^2}{4\hat{n}k_BT}\frac{\partial}{\partial(\omega^2)}G'(\omega)\bigg|_{\omega=0}. \tag{44}$$

The contribution of the finite clusters to the sum in Eq. (41) can be determined based on Eq. (34) by having $\phi(x)$ expressed as a power series in λ:

$$\phi(x)=\sum_{k=0}^{\infty}\lambda^k\phi_k(x). \tag{45}$$

Inserting Eq. (45) in Eq. (33) one has the following for the lowest order term $\phi_0(x)$:

$$\phi_0(x)=q+pe^{-x}\{\phi_0(x)\}^{f-1}. \tag{46}$$

As shown in Appendix C this can be used to calculate ρ_0:

$$\rho_0=\frac{1}{2(f-2)p}[q^2-\{(2-f)\phi_0(0)+(f-1)q\}^2]. \tag{47}$$

Below p_c we have $\phi_0(0)=1$ and from Eq. (47) it follows that ρ_0 is

$$\rho_0=1-\frac{f}{2}p. \tag{48}$$

On the other hand, above p_c Eq. (47) is still valid, but we have to insert for $\phi_0(0)$ the solution of Eq. (46) which at $x=0$ tends to 0 for $p\to 1$.

As shown in Appendix C the inverse moment R_0 can be determined along lines similar to ρ_0, leading to

$$R_0=\frac{f\langle\mu^{-1}\rangle_\mu}{2p}\int_q^{\phi_0(0)} d\phi\frac{(q-\phi)\phi}{(2-f)\phi+(f-1)q}. \tag{49}$$

Different from ρ_0, to which only finite clusters contribute, above p_c the infinite cluster contributes to R_0; this is not included in Eq. (49). On the other hand, Eq. (49) contains also above p_c the correct contribution of the *finite* clusters.

Performing the integration and setting $\phi_0(0)=1$ we obtain the following below p_c:

$$R_0=\langle\mu^{-1}\rangle_\mu\frac{f(f-1)}{2(f-2)^2}\times\left[\frac{f}{2(f-1)}p+\frac{q^2}{p(f-2)}\ln\frac{q}{1-(f-1)p}-1\right]. \tag{50}$$

Together with Eq. (43) this implies that η diverges logarithmically at the percolation threshold $p=1/(f-1)$. In the limit $f\to\infty$ with $2c=pf$ fixed Eq. (50) takes the form

$$R_0=\frac{1}{4c}\left[\ln\left(\frac{1}{1-2c}\right)-2c\right]\langle\mu^{-1}\rangle_\mu. \tag{51}$$

In this way we recover the result, Eq. (37) of Ref. [26], valid for the random graph.

C. Integration for a special distribution

As shown in Ref. [26], the analytical work simplifies considerably for the following distribution of bond strengths:

$$D(\mu)=\frac{1}{\mu^2}\exp(-1/\mu), \tag{52}$$

since for it the operator $\hat{\mathbf{O}}$, Eq. (32), takes the form

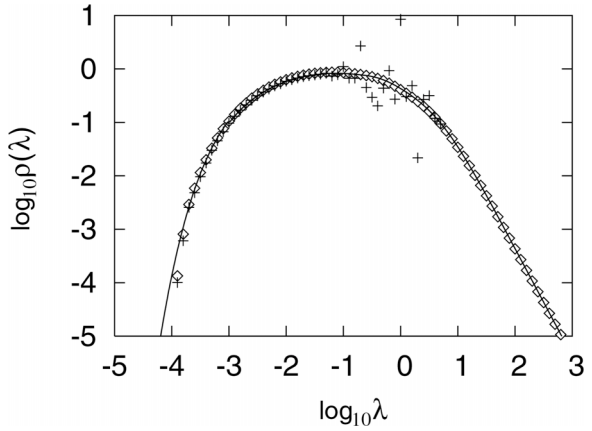

FIG. 1. The density of states $\rho(\lambda)$ in double-logarithmic scales. Displayed are numerically determined spectra for hyperbranched polymers for $f=3$ and $p=0.45$, which are compared to the theoretical results of Sec. III C based on Eq. (54). The numerically determined spectra are (i) for $\mu=1$ (crosses), and (ii) for μ random, obeying Eq. (52) (diamonds). See text for details.

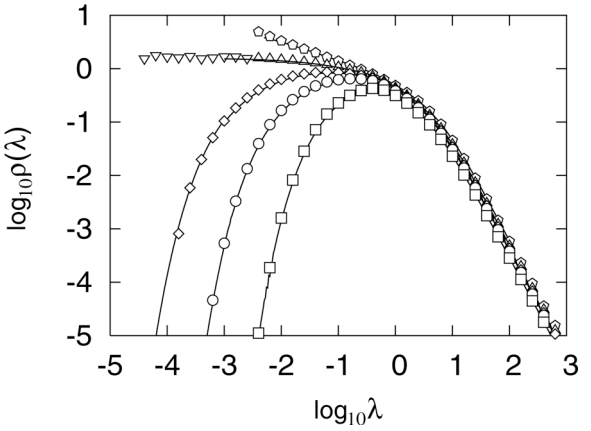

FIG. 2. Same as in Fig. 1 for the $D(\mu)$ distribution of Eq. (52). The theoretical curves are based on Eq. (54). Here $f=3$ and p varies, being $p=0.3$ (squares), 0.4 (circles), 0.45 (diamonds), 0.5 (triangles), and 0.6 (pentagons) from below. For $p=0.5$ the results are obtained for $N_{\max}=500$ (upwards pointing triangles) and 4000 (downwards pointing triangles). All other data are for $N_{\max}=500$.

$$\hat{\mathbf{O}}=\int_0^\infty d\mu\,\frac{1}{\mu^2}\exp(-1/\mu)\exp\left[-\frac{\lambda}{\mu}x\partial_x^2\right]=[1+\lambda x\partial_x^2]^{-1}. \tag{53}$$

For instance, applying $1+\lambda x\partial_x^2=\hat{\mathbf{O}}^{-1}$ to both sides of Eq. (33), one obtains the ordinary second-order differential equation

$$\phi(x)+\lambda x\partial_x^2\phi(x)=q+pe^{-x}\{\phi(x)\}^{f-1}. \tag{54}$$

We expect, as noted in Ref. [26], that the particular choice of $D(\mu)$, Eq. (52), does not change much the small λ behavior of $\rho(\lambda)$, given that in Eq. (52) the probability for small coupling strengths μ is exponentially small. This finding is corroborated by Fig. 1, where we display the density of states $\rho(\lambda)$ obtained from the direct diagonalization of random matrices, as described in the following section. Figure 1 shows the results obtained for $\mu=1$ and for μ obeying Eq. (52); moreover it displays the theoretical result, obtained by solving Eq. (54), as we proceed to do in the following. For large λ (as discussed in Appendix D) one obtains analytically that $\rho(\lambda)$ obeys

$$\rho(\lambda)\simeq fp\lambda^{-2}, \tag{55}$$

as is also evident from Fig. 1. Now, as discussed in Appendix A, Eq. (54) has to be solved subject to the boundary conditions

$$\phi(0)=1 \quad \text{and} \quad \phi(\infty)=q. \tag{56}$$

Formally now, Eqs. (34) and (17) would allow to determine $\rho(\lambda)$. However, we have to calculate $R(\lambda+i\epsilon)$ in the limit $\epsilon\to+0$. For large x the term containing the exponential in Eq. (54) can be neglected; inserting in the remaining form the expression $q+cx^\beta\exp(c'x^\alpha)$ the constants α, β, and c' can be determined, leading to the following result valid for large x:

$$\phi(x)\simeq q+cx^{1/4}\exp\left(-i\sqrt{\frac{x}{\lambda}}\right), \tag{57}$$

where c is still undetermined. In the limit $\epsilon\to0$, Eq. (57) does not fulfill the boundary condition at $x=\infty$, since it oscillates in undamped fashion. One can avoid this problem by rotating the integration contour in Eq. (34):

$$\begin{aligned}R(\lambda)&=-\frac{1}{\lambda}\int_0^{e^{i\psi}\infty}dx\,e^{-x}\{\phi(x)\}^f\\&=-\frac{1}{\lambda}\int_0^\infty dx\,\exp(i\psi-e^{i\psi}x)\{\tilde{\phi}(x)\}^f,\end{aligned} \tag{58}$$

where $\tilde{\phi}(x)\equiv\phi(e^{i\psi}x)$ is obtained from the solutions of

$$\tilde{\phi}(x)+\lambda e^{-i\psi}x\partial_x^2\tilde{\phi}(x)=q+p\,\exp(-e^{i\psi}x)\{\tilde{\phi}(x)\}^{f-1}. \tag{59}$$

Under this transformation, one has the following from Eq. (57) for large x:

$$\tilde{\phi}(x)\simeq q+ce^{i\psi/4}x^{1/4}\exp\left(-ie^{i\psi/2}\sqrt{\frac{x}{\lambda}}\right). \tag{60}$$

Therefore, for $-\pi/2<\psi<0$ and positive real λ it is possible to obtain a solution $\tilde{\phi}(x)$ that fulfills the boundary condition $\phi(\infty)=q$ of Eq. (56).

We stop to note that the results for the density of states obtained via Eq. (58) and the solution of Eq. (59) are independent of the phase ψ. However, the numerical integration of Eq. (59) can be simplified considerably by letting ψ depend on λ and adjusting it. We found empirically that $\psi=-\sqrt{\lambda}\,\pi/3$ for $\lambda\leqslant1$ and $\psi=-\pi/3$ for $\lambda>1$ are good choices.

We are still faced with a nonlinear boundary value problem. This problem can be solved numerically with the

help of standard integration subroutines implemented in MATHEMATICA, as described in Appendix E.

The density of states determined in this way is displayed in Fig. 2 for various values of p. Below the percolation threshold $p=p_c$, it is easy to obtain $\rho(\lambda)$ for quite small values of λ. This changes above $p=p_c$, where an infinite cluster emerges; then, exemplarily, for $p=0.6$ we can obtain $\rho(\lambda)$ for $\lambda \geqslant 10^{-2.2}$. Here the λ values are too large to allow the determination of the small λ behavior of $\rho(\lambda)$ (see the discussion in Sec. V).

IV. NUMERICAL STUDIES

As a support of the integral equation approach discussed above, we have performed independent numerical evaluations; among these we have also determined the spectra through numerical diagonalizations of sets of disordered hyperbranched structures.

A. Regular structures

First, we have checked numerically the consequences of Eq. (31) for finite regular structures of branching functionality f and given generation g. These structures represent the well known dendrimers. Now, the eigenvalue spectra of dendrimers are known to high accuracy, based on exact relations [1,10] derived using the high symmetry of the corresponding **C** matrix. Here we evaluated, for $p=1$ and $\mu=1$, $\phi^{(g)}$ recursively, as given in Eq. (31); we then analyzed the resulting $R^{(g)}$, Eq. (30), in terms of the following sum of partial fractions:

$$R^{(g)}(\lambda)=\sum_j \frac{m_j}{\lambda-\lambda_j}, \tag{61}$$

given that for a single structure and $\mu=1$ the density of states $\rho(\lambda)$ is a sum of δ peaks, so that Eq. (41) turns into Eq. (61). We have confirmed numerically for $f=3$ and $g=5$ (using MATHEMATICA) that this decomposition indeed results from the given $R^{(g)}$ and leads to the known eigenvalues λ_j and multiplicities m_j of the corresponding dendrimer.

B. Random branched structures $p<1$

To numerically calculate the eigenvalue spectra of random branched polymers we have performed extensive numerical diagonalizations. Here, we focused on structures with $f=3$ and explored the eigenvalue spectra for various values of the bond probabilities.

We create our random structures along the procedure outlined in Sec. II by which hyperbranched structures of arbitrary size may be generated. Due to limitations of computer memory and time needed for the subsequent diagonalizations, we restrict the number of bonds of every structure to a maximum of $N_{\max}$, i.e., we stop the procedure as soon as $N_{\max}$ bonds have been created. In general we use $N_{\max}=500$. For $p=0.3$ and 0.4, in 10^{10} attempts this limit was never reached. For the bond probability $p=0.45$, the limit was reached in 10^5 out of 10^9 attempts. To check the reliability of the so-obtained results we also sampled additional structures, by varying $N_{\max}$ and letting it be $N_{\max}=200$, 1000, and 4000. The so-obtained numerical results for $\log_{10}\rho(\lambda)$ agree for $p\leqslant 0.45$ within 5% for the whole range displayed in Fig. 2. For $p=0.5$ and 0.6 we identified for the same percentage value the range of the spectrum that is unaffected by artifacts generated due to the cutoff condition in the recursion algorithm; this region is given by $\lambda \geqslant 10^{-2.2}$.

For each bond of a random branched structure we chose a bond strength μ with distribution $D(\mu)$ as given in Eq. (52). The connectivity matrix $\mathbf{A}_{ij}$ with entries weighted by these bond strengths μ is by construction a real symmetric matrix. We obtained the eigenvalues using a combination of the Householder method and the tridiagonal QL algorithm for diagonalization [36,37].

We have accumulated the eigenvalues of all structures generated for a specific value of the bond probability p, where eigenvalues stemming from a structure with $|S|$ monomers are weighted with a factor of $1/|S|$ to obtain the proper weights, as given by Eqs. (4) and (16). The results of this procedure were already shown in Figs. 1 and 2. In Fig. 2 the corresponding curves for $p=0.5$ and $p=0.6$ have been limited to the range that remains unaffected within 5% by the cutoff at $N_{\max}=500$, i.e., $\lambda>1/N_{\max}$. This can be seen by comparing the results found for $N_{\max}=500$ and 4000 for $p=0.5$ shown in Fig. 2. For $p=0.5$ the number of different realizations used were 8×10^7 and 1.7×10^5 for $N_{\max}=500$ and 4000, respectively. For $p=0.3$, 0.4, 0.45, 0.5, and 0.6 with $N_{\max}=500$ the total number of realizations used was 1.1×10^{10}, 5.0×10^{10}, 8.3×10^9, 8.5×10^7, and 1.1×10^7, respectively, while out of these the number of structures having exactly $N=50$ bonds turned out to be around 1.3×10^4, 2.6×10^7, 1.5×10^7, 1.9×10^5, and 1.6×10^3, respectively.

V. DISCUSSION

As stressed in Sec. II, from the density of states $\rho(\lambda)$ one can evaluate various quantities of physical importance. We obtained $\rho(\lambda)$ both by a numerical treatment of the differential equation (59) and also by a direct approach via the numerical diagonalization of many realizations, as described in Sec. IV B.

First we focus on the stretching of GGSs under external fields [5,6,26,38]. Starting point is Eq. (6). Choosing now the direction of the field along the y axis, $\mathbf{F}=F\mathbf{e}_y$, the stretching is given by

$$\begin{aligned}\langle \delta Y(t)\rangle &= \langle \overline{r_y(t)-r_y(0)}\rangle - F\rho_0 t/\zeta \\ &= \frac{F}{K}\int_0^\infty d\lambda\, \rho_+(\lambda)\frac{1-\exp(-\lambda t/\tau)}{\lambda},\end{aligned} \tag{62}$$

where the average extends now also over the distinct realizations of the hyperbranched structures. In Fig. 3 we plot in double-logarithmic scales the dimensionless quantity $\langle \delta\hat{Y}\rangle = \langle \delta Y\rangle K/F$ against the dimensionless time $\hat{t}=t/\tau$ for various values of p.

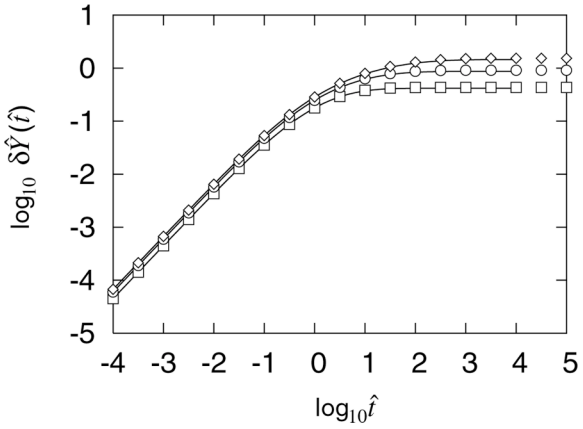

FIG. 3. The averaged dimensionless stretching, Eq. (62), plotted in double-logarithmic scales against the dimensionless time $\hat{t} = t/\tau$, see text for details. The results are obtained from the analytical and numerical $\rho(\lambda)$ data displayed in Fig. 2. The bond probabilities are $p = 0.3$, 0.4, and 0.45, from below.

Quantities of special experimental importance are the storage modulus G' and the loss modulus G'', which we evaluated with the help of Eqs. (11) and (12). We display both the moduli and the angular frequency ω in dimensionless units ($\hat{\omega} = \omega/\tau$, $\hat{G}' = G'/\hat{n}k_BT$, and $\hat{G}'' = G''/\hat{n}k_BT$) in double-logarithmic scales in Figs. 4 and 5. Classically and independent of the considered structure, for very small ω values $G'(\omega)$ increases quadratically in ω, whereas $G''(\omega)$ shows a ω dependence. For very large ω, on the other hand, $G'(\omega)$ reaches a plateau, which following Eq. (48) should be $\hat{n}k_BTpf/2$, whereas $G''(\omega)$ decays as ω^{-1}. The small ω behavior, especially in the case of $G'(\omega)$, is not attained, see Fig. 5. In all cases the prefactors are dominated by small eigenvalues, being related to the inverse moments of $\rho_+(\lambda)$ via Eqs. (44) and (43). One may naively expect, based on Eq. (55), that $G''(\omega)$ should vanish like $\omega^{-1}\ln\omega$ in the high frequency limit. We do not detect such a logarithmic dependency in Fig. 5. Moreover, the logarithm may be an artifact, due to the presence of large μ values in Eq. (55). In the region between the small and large ω regimes the behavior of $G'(\omega)$ and $G''(\omega)$ is characteristic of the underlying structures. Here we observe rather smooth curves. This is caused by the vast number of different hyperbranched structures with bonds of different strengths, which all contribute to $G'(\omega)$ and $G''(\omega)$, and differs from the cases of single dendrimers or of hyperbranched structures with a fixed number of monomers [7]. In these cases one recognizes at intermediate ω in the behavior of $G'(\omega)$ and $G''(\omega)$ the signature of the underlying structures; thus in Refs. [5,6] doubly logarithmic displays of $G'(\omega)$ and $G''(\omega)$, such as in Figs. 4 and 5, disclosed for dendrimers a logarithmic-type behavior, which is related to their exponential growth with g.

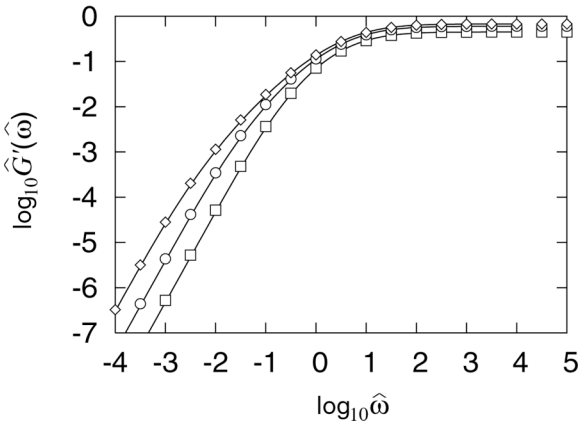

FIG. 4. The dimensionless storage modulus $\hat{G}'(\hat{\omega})$ plotted in double-logarithmic scales against the dimensionless frequency $\hat{\omega} = \omega/\tau$, see text for details. The results are obtained from the analytical and numerical $\rho(\lambda)$ data displayed in Fig. 2. The bond probabilities are $p = 0.3$, 0.4, and 0.45, from below.

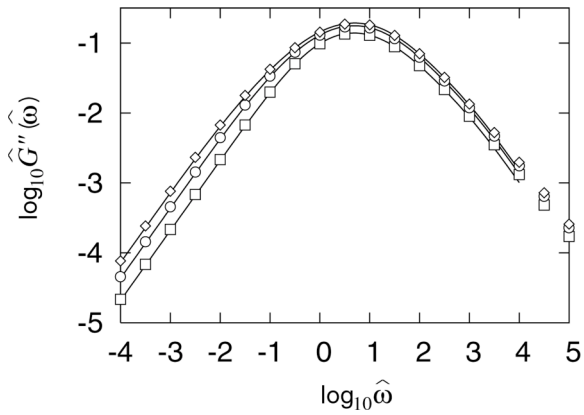

FIG. 5. Same as Fig. 4 for the dimensionless loss modulus $\hat{G}''(\hat{\omega})$.

In Figs. 3–5 the differences between the analytical and the numerical diagonalization results are quite small and hence hardly observable; this is due to the fact that $\langle \delta Y(t) \rangle$, $G'(\omega)$, and $G''(\omega)$ do not test the small λ range in detail. We now turn to discuss aspects for which the small λ range is important. In the random graph case heuristic arguments have been given [25,26] for the existence of a Lifschitz tail in the density of states. One expects the form

$$\rho_+(\lambda) \sim \exp\left[-\frac{A(p)}{\sqrt{\lambda}}\right], \quad \lambda \to 0, \tag{63}$$

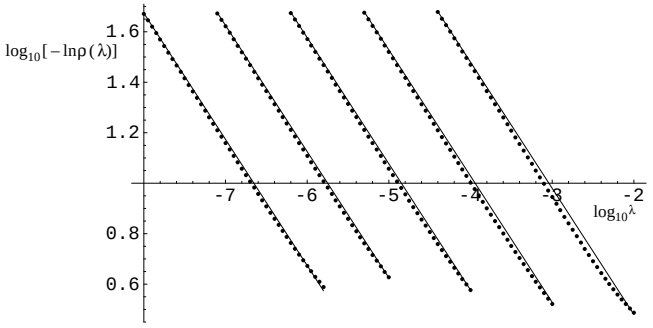

FIG. 6. Results for the Lifshitz tail of $\rho(\lambda)$ for different p, obtained from integrating Eq. (59) (dots). The results are compared with Eq. (63) (straight lines) for a fitted A_0 value, $A_0 = 3.375$. Here $p = 0.4$, 0.45, 0.475, 0.4875, and 0.493 75 from left to right.

where $A(p) \sim A_0(p-p_c)^{3/2}$ for $p \to p_c$. This behavior stems from the fact that small eigenvalues are produced by large linear regions occurring with small probability. If p approaches p_c the probability of these large linear structures increases, resulting in a finite density of states for $\lambda \to 0$ at p_c. In Fig. 6 we plotted $\log_{10}[-\ln \rho(\lambda)]$ obtained from the integration of Eq. (59) against $\log_{10}\lambda$ in comparison with form (63) for values of $\rho(\lambda)$ down to 10^{-19} and p values close to but smaller than $p_c = 1/2$. The agreement between the analytical results and Eq. (63) is nice, when we take for A_0 the value $A_0 = 3.375$. Note that in our direct diagonalization calculations we did not reach the small λ range explored here by the analytic approach: For instance we did not obtain, say for $p = 0.45$, eigenvalues lower than $\lambda = 10^{-4}$, see Fig. 1.

Above the percolation threshold $p = 1/2$ large linear regions become rare again, since then the structures get more branches. Unfortunately, we are not able to reach the small λ regime above p_c (see, for instance, our Fig. 2 for the case $p = 0.6$), where a behavior such as Eq. (63) could again be observed.

Inserting Eq. (63) into Eq. (62) we obtain the following, analogously to Ref. [38], for large t:

$$\langle \delta Y(t) \rangle \sim \frac{F}{K} \int d\lambda \, \exp\left[-\frac{A(p)}{\sqrt{\lambda}} \right] \frac{1-\exp(-\lambda t/\tau)}{\lambda}. \tag{64}$$

The integral may be evaluated through a saddle-point approximation, giving

$$\langle \delta Y(t) \rangle \sim \frac{F}{K} \left(\frac{2\eta}{k_B T \tau} - c_1 t^{\gamma'} \exp\left[-\left\{ \frac{3A(p)}{2} \right\}^{2/3} \left(\frac{t}{\tau} \right)^{1/3} \right] \right), \tag{65}$$

where c_1 is a constant. Due to the dependence of $A(p)$ on p it follows that $\langle \delta Y(t) \rangle$ is quite sensitive to p near $p_c = 1/2$.

VI. CONCLUSIONS

This work was devoted to the dynamics of randomly hyperbranched polymers in the framework of a Rouse-type approach. In such an approach, the fundamental quantity for the dynamics is the density of states, see Eqs. (6), (11), and (12) as well as Refs. [5,6,26]. In former works on general hyperbranched polymers the ensemble averaged density of states had been computed using numerical diagonalization techniques [7,23]. In parallel to these techniques, we used here the replica method to evaluate the ensemble average over disordered structures; we obtained in this way an integral equation for the density of states $\rho(\lambda)$. The results of the two approaches are in convincing agreement for a large range of λ. From the data of $\rho(\lambda)$ various quantities of physical interest, i.e., the stretching and the storage and loss moduli G' and G'', could be numerically evaluated.

Besides the intrinsic interest of having an analytic method, the main advantage of the replica approach appears if one focuses on the long-time dynamics of structures close to the percolation threshold. This regime is governed by very low lying eigenfrequencies, which are mainly due to structures displaying large quasilinear regions or having very weak bonds. Such situations are rare and therefore difficult to monitor in an approach based on direct numerical diagonalization. On the other hand, the analytic approach could reflect them; it allowed us, for instance, to treat the question of the appearance of Lifschitz tails in the density of states.

ACKNOWLEDGMENTS

The support of the DFG, of the BMBF, and of the Fonds der Chemischen Industrie are gratefully acknowledged.

APPENDIX A: DETAILS OF THE $n \to 0$ LIMIT

The $n \to 0$ limit is performed as shown in Ref. [26], by using the integral representation of the n-dimensional Laplacian

$$\int d\mathbf{r}' \exp\left[-i\frac{\mu}{2}(\mathbf{r}-\mathbf{r}')^2 \right] f(|\mathbf{r}'|) = (2\pi/i\mu)^{n/2} \times \exp\left[\frac{1}{2i\mu} \left(\partial_\rho^2 + \frac{n-1}{\rho} \partial_\rho \right) \right] f(\rho)_{\rho=|\mathbf{r}|}, \tag{A1}$$

which is valid for rotationally invariant functions $f(|\mathbf{r}|)$.

From the structure of Eqs. (26) and (29) it follows iteratively that $\hat{\phi}^{(g)}(\mathbf{r})$ depends only on $r \equiv |\mathbf{r}|$. Therefore given the relation

$$\lim_{n\to 0} \int d\mathbf{r} f(r) = \lim_{n\to 0} \frac{2\pi^{n/2}}{\Gamma(n/2)} \int_0^\infty dr \, r^{n-1} f(r) = f(0), \tag{A2}$$

valid for any rotationally invariant function $f(r)$, one has from Eq. (28) for $n \to 0$

$$R^{(g)}(\lambda) = i \int_0^\infty dr \, r \exp\left[i\frac{\lambda}{2} r^2 \right] \{\hat{\phi}^{(g)}(r)\}^f. \tag{A3}$$

On the other hand, one has the following from Eqs. (A1), (A2), and (29):

$$\hat{\phi}^{(g)}(r) = q\hat{\phi}^{(g-1)}(0) + p \int_0^\infty d\mu \, D(\mu) \times \exp\left[\frac{1}{2i\mu} \left(\partial_r^2 - \frac{1}{r}\partial_r \right) \right] \exp\left[i\frac{\lambda}{2} r^2 \right] \times \{\hat{\phi}^{(g-1)}(r)\}^{f-1}. \tag{A4}$$

Introducing the function $\phi(x) \equiv \hat{\phi}(r[x])$ with $r[x] \equiv \sqrt{2ix/\lambda}$ and using the relation

$$\lambda x \partial_x^2 f(r[x]) = i\left(\frac{1}{2}\partial_r^2 - \frac{1}{2r}\partial_r \right) f(r[x]) \tag{A5}$$

for an arbitrary function $f(r)$ we obtain Eqs. (30) and (31).

From $\phi^{(0)}(0)=1$ and Eqs. (31) and (32) we conclude that $\phi^{(g)}(0)=1$ is valid for all generations g regardless of the value of q. Hence it is also valid for the whole Cayley tree. In the same fashion the property $\phi^{(g)}(\infty)=q$ follows from Eq. (A4) for all λ with a small positive imaginary part. We stop to note that we have just obtained the boundary conditions, Eq. (56) of the main text.

APPENDIX B: PROOF OF THE PROPERTY, EQ. (37)

To establish Eq. (37) we note that the functions

$$\psi_\alpha(x)=\sum_{k=1}^{\infty}\frac{\alpha^{k-1}}{k!(k-1)!}x^k \tag{B1}$$

fulfill

$$x\partial_x^2\psi_\alpha(x)=\alpha\psi_\alpha(x), \tag{B2}$$

i.e., are eigenfunctions of the operator $x\partial_x^2$ to the eigenvalue α. It is straightforward to verify the relation

$$\int_0^\infty d\alpha\psi_\alpha(x)e^{-\alpha/a}=\sum_{k=1}^{\infty}\frac{1}{k!}a^kx^k=e^{ax}-1, \tag{B3}$$

via term by term integration. This can be used to determine the action of $\exp[-\lambda x\partial_x^2]$ on e^{ax}:

$$\begin{aligned}\exp[-\lambda x\partial_x^2]e^{ax}&=\exp[-\lambda x\partial_x^2]\left(1+\int_0^\infty d\alpha\psi_\alpha(x)e^{-\alpha/a}\right)\\&=1+\int_0^\infty d\alpha e^{-\lambda\alpha}\psi_\alpha(x)e^{-\alpha/a}=e^{x/(\lambda+1/a)},\end{aligned} \tag{B4}$$

where in the last step we used again Eq. (B3). Rearranging the right-hand side of Eq. (B4) results in Eq. (37) of the main text.

APPENDIX C: LOW FREQUENCY EXPANSION

The quantity ρ_0 is entirely determined by $\phi_0(x)$, see Eqs. (34), (41), and (45). We now make use of the relation

$$\phi_0'=-pe^{-x}\frac{\phi_0^f}{(2-f)\phi_0+(f-1)q}, \tag{C1}$$

where the prime denotes the derivative with respect to x. Equation (C1) follows by differentiating and rearranging Eq. (46). From Eq. (C1) we obtain for the weight of the zero eigenvalue

$$\rho_0=\int_0^\infty dx\,e^{-x}\phi_0^f=-\frac{1}{p}\int_0^\infty dx\,\phi_0'[(2-f)\phi_0+(f-1)q], \tag{C2}$$

from which Eq. (47) follows by performing the integration. To evaluate Eq. (47) one has to choose a specific solution of Eq. (46) to determine $\phi_0(0)$. To cope with this, we note that from Eq. (46) one has the following expansion in powers of $pq^{f-2}e^{-x}$:

$$e^{-x}\{\phi_0(x)\}^f=q^f\sum_{k=1}^{\infty}a_kp^{k-1}q^{(k-1)(f-2)}e^{-kx}. \tag{C3}$$

Inserting this into Eq. (47) we obtain

$$\rho_0=q^f\sum_{k=1}^{\infty}\frac{1}{k}a_kp^{k-1}q^{(k-1)(f-2)}. \tag{C4}$$

On the other hand, one obtains from Eq. (15)

$$\rho_0=\sum_{|S|=1}^{\infty}\frac{1}{|S|}W_{|S|}, \tag{C5}$$

where $W_{|S|}=\Sigma_{S,S=|S|}w_S$ is the probability that a monomer belongs to a cluster of $|S|$ monomers. Finally from the observation that $W_{|S|}$ contains the factor $p^{|S|-1}q^{|S|(f-2)+2}$ the identification

$$a_kp^{k-1}q^{k(f-2)+2}=W_k \tag{C6}$$

follows. A statement similar to Eqs. (C3) and (C6) was given in Ref. [39]. Thus the total probability that a monomer is contained in a finite cluster is given by $\{\phi_0(0)\}^f$ and one has to choose the solution of Eq. (46) that is unity for $x=0$ and $p<p_c$.

As an illustration of these findings we consider the case $f=3$, where the solution of Eq. (46) with the desired properties is

$$\phi_0(x)=\frac{e^x}{2p}(1-\sqrt{1-4pqe^{-x}}). \tag{C7}$$

This gives indeed $\phi_0(0)=1$ for $p<p_c=1/2$. On the other hand, one has $\phi_0(0)=1/p-1$, which in view of Eq. (C3) reflects the fact that above the percolation threshold we have the finite probability $1-(1/p-1)^3$ that a monomer is contained in the infinite cluster.

From Eqs. (34) and (45) we remark that R_0 can be calculated based on the knowledge of $\phi_0(x)$ and $\phi_1(x)$. Inserting Eq. (45) into Eq. (33) we obtain from the linear term in λ

$$pe^{-x}\phi_0^{f-1}\phi_1=-x\phi_0'\phi_0''\langle\mu^{-1}\rangle_\mu. \tag{C8}$$

This relation allows now to determine R_0:

$$\begin{aligned}-R_0&=f\int_0^\infty dx\,e^{-x}\phi_0^{f-1}\phi_1\\&=-\frac{f\langle\mu^{-1}\rangle_\mu}{p}\int_0^\infty dx\,x\phi_0'\phi_0''=\frac{f\langle\mu^{-1}\rangle_\mu}{2p}\int_0^\infty dx\,(\phi_0')^2\\&=-\frac{f\langle\mu^{-1}\rangle_\mu}{2p}\int_0^\infty dx\frac{(\phi_0-q)\phi_0}{(2-f)\phi_0+(f-1)q}\phi_0',\end{aligned} \tag{C9}$$

from which Eq. (49) follows.

APPENDIX D: LARGE λ BEHAVIOR

To obtain the large λ behavior of $\rho(\lambda)$, we make the substitution $\phi(x)\rightarrow\phi(x/\lambda)$; Eq. (54) takes then in the limit $\lambda\rightarrow\infty$ the form

$$\phi_\infty(x)+x\phi_\infty''(x)=q. \tag{D1}$$

Introducing the function $K_1(x)$ via

$$\phi_\infty(x)=q+2pi\sqrt{x}K_1(2i\sqrt{x}), \tag{D2}$$

Eq. (D2) turns into Bessel's differential equation for $K_1(x)$, Eq. (8.494) of Ref. [40]:

$$\partial_x^2K_1(x)+\frac{1}{x}\partial_xK_1(x)-\left(1+\frac{1}{x^2}\right)K_1(x)=0. \tag{D3}$$

Then taking into account the boundary conditions, Eq. (56), $K_1(x)$ can be identified with the modified Bessel function of the first kind. Using the small x expansion of $K_1(x)$, Eq. (8.446) of Ref. [40], we obtain

$$\mathrm{Im}\{\phi_\infty(x)\}^f=\pi fpx+O(x^2), \tag{D4}$$

and inserting this into the expression

$$\rho(\lambda)=\frac{1}{\pi}\frac{1}{\lambda}\mathrm{Im}\int_0^\infty dxe^{-x}\{\phi(x/\lambda)\}^f \tag{D5}$$

for the density of states, we obtain Eq. (55).

APPENDIX E: SOLUTION OF THE NONLINEAR BOUNDARY VALUE PROBLEM

We restrict the discussion here to the case $f=3$, since the generalization to arbitrary values of f is straightforward. To solve the nonlinear boundary value problem given by Eq. (59) we first integrate Eq. (59) using the subroutine NDSolve of MATHEMATICA with the initial values $\phi(\infty)=q$, $\phi'(\infty)=0$. This leads to a solution $\phi_i(x)$ which differs from 1 at $x=0$. Therefore we have to add a second solution $\phi_h(x)=\phi(x)-\phi_i(x)$, obeying the equation

$$\phi_h(x)+\lambda e^{-i\psi}x\partial_x^2\phi_h(x)=p\exp(-e^{i\psi}x)\{2\phi_i(x)+\phi_h(x)\}\phi_h(x), \tag{E1}$$

which is complemented with the boundary conditions

$$\phi_h(0)=1-\phi_i(0)\quad\text{and}\quad\phi_h(\infty)=0. \tag{E2}$$

The solution to Eq. (E1) is obtained recursively. In the first step we linearize Eq. (E1) by neglecting the term quadratic in $\phi_h(x)$. To obtain $\phi_h^k(x)$ of the kth recursion step we linearize Eq. (E1) by inserting the solution $\phi_h^{k-1}(x)$ of the last step in the curly brackets of the right-hand side, which leads to the iteration scheme

$$\phi_h^k(x)+\lambda e^{-i\psi}x\partial_x^2\phi_h^k(x)=p\exp(-e^{i\psi}x)\{2\phi_i(x)+\phi_h^{k-1}(x)\}\phi_h^k(x). \tag{E3}$$

These linear equations are integrated with the initial values

$$\phi_h^{k\prime}(x_m)=\phi_h^{k-1\prime}(x_m)\quad\text{and}\quad\phi_h^k(x_m)=0, \tag{E4}$$

where x_m is a large number, adjusted to maximize numerical precision. After each iteration step the solution $\phi_h^k(x)$ is normalized according to the first of the conditions, Eq. (E2), i.e., $\phi_h^k(0)=1-\phi_i(0)$. Note that it is important to integrate Eq. (C8) from $x=\infty$ to $x=0$, since otherwise rounding errors would always produce an exponentially growing solution. It turns out that within this procedure the solution converges rapidly after a few iteration steps. Especially for $\lambda\ll1$, the solution is obtained with sufficient accuracy after the first iteration step, if p lies below the percolation threshold.

[1] C. Cai and Z.Y. Chen, Macromolecules **30**, 5104 (1997).
[2] Z.Y. Chen and C. Cai, Macromolecules **32**, 5423 (1999).
[3] F. Ganazzoli, R. La Ferla, and G. Raffaini, Macromolecules **34**, 4222 (2001).
[4] A.A. Gurtovenko and A. Blumen, J. Chem. Phys. **115**, 4924 (2001).
[5] P. Biswas, R. Kant, and A. Blumen, Macromol. Theory Simul. **9**, 56 (2000).
[6] P. Biswas, R. Kant, and A. Blumen, J. Chem. Phys. **114**, 2430 (2001).
[7] C. von Ferber and A. Blumen, J. Chem. Phys. **116**, 8616 (2002).
[8] R.L. Ferla, J. Chem. Phys. **106**, 688 (1997).
[9] R. Kant, P. Biswas, and A. Blumen, Macromol. Theory Simul. **9**, 608 (2000).
[10] A.A. Gurtovenko, Y.Y. Gotlib, and A. Blumen, Macromolecules **35**, 7481 (2002).
[11] J. Roovers, in *Star and Hyperbranched Polymers*, edited by M. K. Mishra and S. Kobayashi (Marcel Dekker, New York, 1996).
[12] J. Roovers and B. Comanita, Adv. Polym. Sci. **142**, 179 (1999).
[13] W. Burchard, Adv. Polym. Sci. **143**, 113 (1999).
[14] J.J. Freire, Adv. Polym. Sci. **143**, 35 (1999).
[15] D.A. Tomalia, A.M. Naylor, and W.A. Goddard, Angew. Chem., Int. Ed. Engl. **29**, 138 (1990).
[16] M.C. Moreno-Bondi, G. Prelana, N.J. Turro, and D. Tomalia, Macromolecules **23**, 910 (1990).
[17] C.J. Hawker and J.M.J. Fréchet, J. Am. Chem. Soc. **112**, 7638 (1990).
[18] C.J. Hawker and J.M.J. Fréchet, Macromolecules **23**, 4726 (1990).
[19] G. R. Newkome, *Advances in Dendritic Macromolecules* (JAI Press, London, 1996).
[20] J.M.J. Fréchet, Science **263**, 1710 (1994).
[21] R. Yin, Y. Zhu, and D.A. Tomalia, J. Am. Chem. Soc. **120**, 2678 (1998).

[22] V. Percec, C.H. Ahn, G. Ungar, D.J.P. Yeardly, M. Möller, and S.S. Sheiko, Nature (London) **391**, 161 (1998).
[23] J. Kemp and Z.Y. Chen, Phys. Rev. E **56**, 7017 (1997).
[24] Y. Kim and A.B. Harris, Phys. Rev. B **31**, 7393 (1985).
[25] A.J. Bray and G.J. Rodgers, Phys. Rev. B **37**, 3557 (1988).
[26] K. Broderix, T. Aspelmeier, A.K. Hartmann, and A. Zippelius, Phys. Rev. E **64**, 021404 (2001).
[27] G. Grimmet, *Percolation* (Springer-Verlag, New York, 1989).
[28] M.E. Fisher and J.W. Essam, J. Math. Phys. **2**, 609 (1961).
[29] D. Ben-Avraham and S. Havlin, *Diffusion and Reactions in Fractals and Disordered Systems* (Cambridge University Press, Cambridge, 2000).
[30] J.-U. Sommer and A. Blumen, J. Phys. A **28**, 6669 (1995).
[31] P.E. Rouse, J. Chem. Phys. **21**, 1272 (1953).
[32] M. Doi and S. F. Edwards, *The Theory of Polymer Dynamics* (Clarendon Press, Oxford, 1986).
[33] H. Yamakawa, *Modern Theory of Polymer Solutions* (Harper and Row, New York, 1971).
[34] M. Mezard, G. Parisi, and M. A. Virasoro, *Spin Glass Theory and Beyond* (World Scientific, Singapore, 1986).
[35] M. Le Bellac, *Quantum and Statistical Field Theory* (Clarendon Press, Oxford, 1997).
[36] W. H. Press, B. P. Flannery, S. A. Teukolsky, and W. T. Vetterling, *Numerical Recipes* (Cambridge University Press, Cambridge, 1990).
[37] J. H. Wilkinson and C. Reinsch, *Linear Algebra, Handbook for Automatic Computation* (Springer, New York, 1971), Vol. 2.
[38] I.M. Sokolov, S. Jespersen, and A. Blumen, J. Chem. Phys. **113**, 7652 (2002).
[39] M.J. Stephen, Phys. Rev. B **17**, 4444 (1978).
[40] I. S. Gradshteyn and I. M. Ryzhik, *Table of Integrals Series and Products* (Academic Press, San Diego, 1980).